Application Note

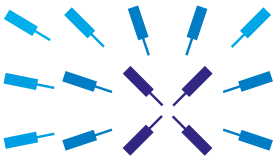

Zurich Instruments

Superconducting Qubit Characterization

Applications: Quantum Computing, Circuit QED
Products: UHFLI, UHF-AWG, UHF-DIG, UHF-MF

Release date: October 2016

Introduction

Quantum Computing

Quantum computing promises an advance in numerical processing power over classical computing by exploiting quantum physical phenomena [1, 2]. Present-day experimental work in this field focuses on improving the devices that ultimately would take over the function of transistors in classical processors: the quantum bits (qubits). Superconducting qubits are among the most promising candidates explored today [3, 4]. Being based on microfabrication technology and purely electrical control, superconducting qubits come with a clear roadmap for large-scale integration of hundreds of qubits in a single processor. The steady improvement of coherence times achieved over recent years inspires confidence that these devices can be engineered to a quality that enables practical numerical algorithms.

Growing Complexity

Controlling superconducting qubits requires complex pulsed microwave signals on multiple channels with precise synchronization. As the number of qubits and channels increases, there is a need for more integrated, standardized, and more reliable electronic control solutions. The Zurich Instruments UHFLI instrument addresses this demand as it combines an arbitrary waveform generator (AWG) for synthesis of precisely shaped pulsed signals, and a 600 MHz lock-in amplifier with digitizer for detection. Combining generation and detection in one instrument reduces setup complexity, improves synchronization, reduces rack space, and enables advanced control methods based on feed-forward from detection to generation, e.g. sequence branching.

Here we describe how to use the UHFLI instrument to characterize superconducting qubits in terms of their frequency, qubit state lifetime and coherence time. The measurements presented also provide tuning of the pulse shapes used to compose quantum computing sequences. The single-qubit device used in the experiments presented here is designed according to the circuit quantum electrodynamics architecture [5] which is extendable towards multi-qubit experiments. The measurements were carried out in Prof. A. Wallraff's Quantum Device Lab at ETH Zurich, Switzerland.

Setup and Sample

Quantum computing devices are designed to enable control and readout of a qubit's quantum state. The quantum state is generally a quantum superposition of two physical configurations of the qubit device which encodes the information processed in a quantum computer. The sample shown in Fig. 1 (a) consists of niobium- and aluminium-based resonant circuits on a sapphire chip. The actual qubit is a nonlinear resonator formed of a small superconducting quantum interference device (SQUID) and an on-chip capacitor (orange in the image). The SQUID design makes the qubit frequency tunable over a frequency range between about 4 and 7.5 GHz by adjusting a small magnetic field applied to the device.

A coplanar waveguide (green) directs external signals directly to the qubit for its control. The qubit is coupled to a coplanar-waveguide resonator (blue) [5] at 4.78 GHz. This readout resonator is connected through an on-chip filter to a pair of coaxial cables that provide the interface for reading out the quantum state of the qubit. Figure 1 (b) depicts a schematic of the measurement setup in which the sample is installed in a dilution refrigerator to provide a well isolated low-temperature environment protecting the quan-

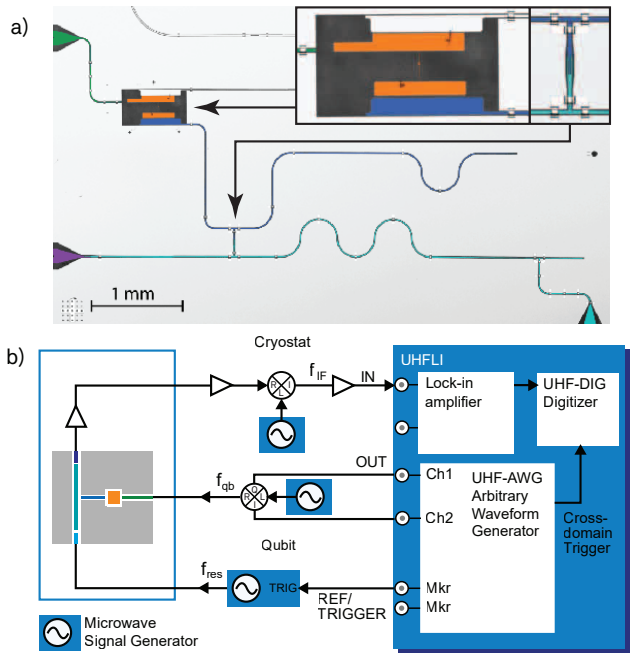

Figure 1. (a) Optical micrograph of the sample showing the readout resonator (blue) and the qubit capacitor plates (orange). The resonator is coupled to input and output lines via a Purcell filter [6] (cyan). Insets show magnified views of the qubit and the coupler between resonator and Purcell filter. (b) Simplified diagram of the experimental setup based on the UHFLI instrument integrating a lock-in amplifier and an AWG. The superconducting qubit sample is cooled in a dilution refrigerator.

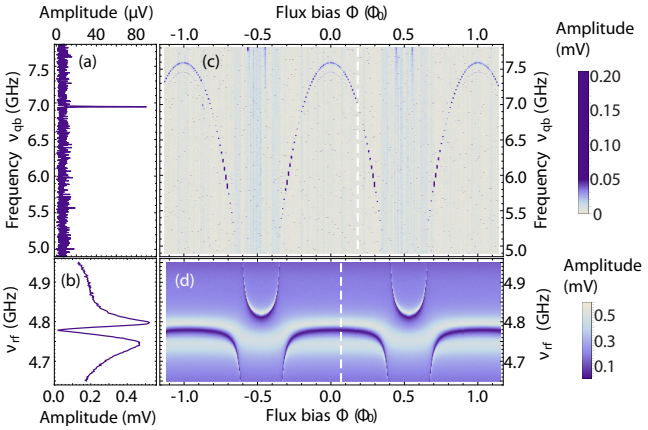

Figure 2. Spectra of the qubit (a) and of the readout resonator (b). The measurement in (a) is obtained by measuring the transmission at a fixed frequency ν_{rf} close to the cavity resonance (b) and sweeping the qubit drive frequency ν_{qb}. (c) The arc-shaped dependence on magnetic flux Φ is characteristic for this type of qubit. As the qubit frequency crosses the frequency of the readout resonator along the horizontal axis in (d), the two exhibit an avoided crossing. The color scale shows the amplitude of the signal transmitted through the readout resonator after amplification.

tum properties of the sample.
The control pulses are generated by quadrature modulation of a microwave signal using two AWG channels. The pulses for qubit readout are generated by feeding one of the AWG marker channels to the gate input of a signal generator. After transmission through the readout resonator, the pulses are amplified and the readout signal is down-converted to an intermediate frequency f_{IF} and measured with one of the UHFLI lock-in amplifier channels.

Measurements

Qubit Spectroscopy

We start with spectroscopic measurements of the frequency and linewidth of the qubit and of the readout resonator. Spectroscopy also allows us to find the optimum magnetic field bias, set by using a small coil at the sample.
For the measurement of the readout resonator, we apply a continuous microwave tone to the resonator and measure the amplitude of the downconverted transmitted signal with the lock-in amplifier. The frequency ν_{res} of that tone is swept across the resonator frequency f_{res}. Such a measurement is shown in Fig. 2 (b). The transmission lineshape of the resonator is a narrow dip at f_{res} on top of a broader peak which is due to the on-chip Purcell filter [6].
For the measurement of the qubit transition frequency, we use a two-tone microwave technique. The first microwave tone is applied to the readout resonator at a fixed frequency close to resonance f_{res}. While measuring the transmission amplitude, a second tone is applied to the qubit gate line and its frequency ν_{qb} is swept across a wide range. Owing to the dispersive coupling between the qubit and the readout resonator, a change in the signal is detected when ν_{qb} becomes resonant with the qubit transition at f_{qb} [5]. This leads to a feature at f_{qb} as seen in Fig. 2 (a).
Figure 2 (c) and (d) shows the qubit and resonator spectra as a function of magnetic field. The qubit transition frequency shows a characteristic, arc-shaped dependence on magnetic field [7]. At specific magnetic fields, the qubit and readout resonator frequencies exhibit an avoided crossing seen in (d). This so-called vacuum Rabi splitting is an effect of the strong coupling between qubit and resonator.
All subsequent measurements are pulsed rather than continuous to probe the dynamic properties of the qubit. The basis of these measurements is a pulse sequence consisting of a control part and a readout part. During the control part we apply pulses to the qubit gate line at a frequency close to f_{qb}. These resonant pulses lead to a coherent oscillation of the qubit between its ground and excited state known as Rabi oscillations. After the control part we apply a pulse to the readout resonator at a frequency close to f_{res} and perform a triggered measurement of the signal after transmission through the sample. To that end, the return signal is first down-converted in the analog domain to f_{IF} = 28.125 MHz, and then demodulated in the digital domain using the lock-in amplifier. Using digital lock-in technology instead of direct down-conversion to DC protects the measurement from amplifier offset voltage drift and 1/f noise [8].
The entire cycle is repeated several thousand times in

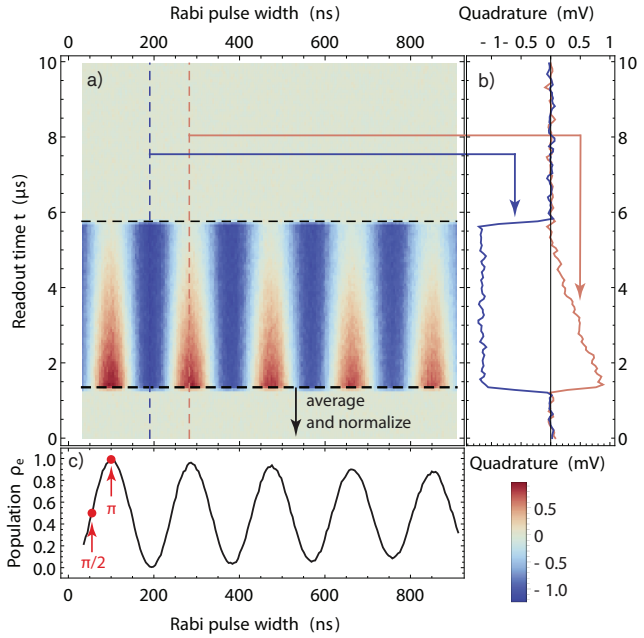

Figure 3. Rabi oscillation measurement. As a function of the width of the control pulse, the qubit evolves periodically from ground state to excited state and back. This results in a sinusoidal readout signal amplitude as a function of the pulse width (horizontal axis) as seen in the color plot in (**a**). (**b**) Time-dependent readout signal at two values of the pulse width marked in (**a**). The time between about 1.2 µs and 5.8 µs corresponds to the readout pulse. (**c**) Rabi oscillation plot obtained by averaging the data in (**a**) and normalizing the result to obtain a mean excited-state population. The measurement allows us to determine the parameters for π- and π/2-pulses (red marks).

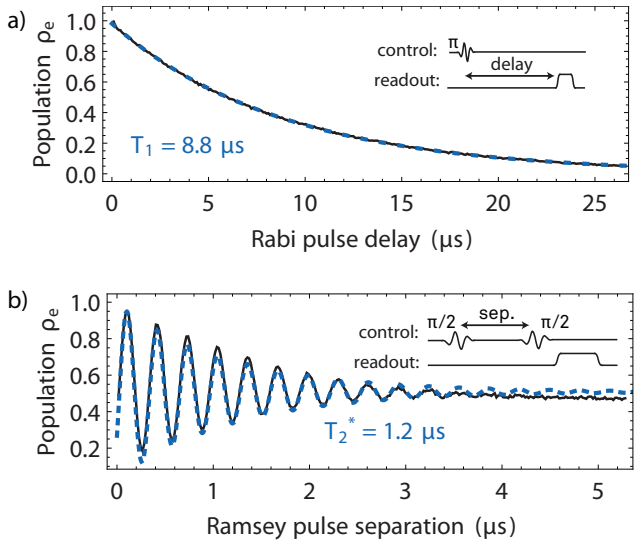

Figure 4. (**a**) Qubit lifetime T_1 measurement. The qubit is initialized in the excited state with a π-pulse. The subsequent exponential decay is then measured for increasing delays before the readout pulse. (**b**) Ramsey fringe measurement. As the delay between two π/2-pulses is varied, the qubit readout signal follows a decaying oscillatory evolution reflecting the gradual loss of phase coherence. The measurement is used to determine the qubit coherence time T_2^*. Both measurements were averaged 40'000 times at a 27 kHz repetition rate.

order to increase signal-to-noise ratio and to average out quantum fluctuations. Conventionally, the down-conversion is performed after averaging the raw data. The UHFLI's digital demodulators enable downconversion before averaging. This method eliminates one data post-processing step from the experiment, and it eliminates the neccessity to choose an intermediate frequency that is commensurate with the repetition rate. Furthermore it is essential when implementing feed-forward protocols where the demodulated signal needs to be available rapidly.

Rabi Oscillations

Applying a control pulse leads to a well-defined change of the qubit state that can be used as a single-qubit gate operation. Such operations are required to implement quantum computing algorithms, in a similar way as for instance the logical inversion is required for classical computing algorithms. A Rabi oscillation measurement allows us to determine the pulse parameters for a given gate operation.

For this measurement we generate a control pulse with an envelope shaped by smooth edges (rise/fall time 3.9 ns) and a flat plateau with a variable width. The control pulse is followed by a readout pulse which is a microwave burst with an approximately rectangular envelope. The qubit's probability for being in the excited state follows a sinusoidal evolution as a function of the control pulse area, which is again proportional to its width at half maximum. This evolution is reflected in the measured signal during the readout phase plotted in Fig. 3. The curve allows us to identify the width of the qubit gate pulses relevant for the next measurements: the so-called π-pulse width corresponds to the first maximum, and the π/2-pulse width corresponds to the first quarter period. The π-pulse brings the qubit from its ground to the excited state, whereas the π/2-pulse brings the qubit to an equal coherent superposition of ground and excited state. For this measurement, every control pulse was repeated 4000 times at a rate of 13 kHz.

Qubit Lifetime

Decay from the excited qubit state to the ground state limits the duration of a computation algorithm. Measuring the average lifetime T_1 is therefore an important part of the device characterization. For a T_1 measurement we apply a π-pulse at the start of a sequence, then wait for a variable time t, and finally measure the qubit state. The resulting data is plotted in Fig. 4 (a). From the fit to an exponential $\exp(-t/T_1)$ we extract the lifetime T_1 = 8.8 µs.

The UHFLI's control software LabOne® is able to generate waveforms and sequences directly. For this measurement, we generated a series of 200 patterns with the UHF-AWG using a sequencer loop incrementing the readout pulse delay from 0 µs to about 26 µs using run-time sequencer variables and dynamic waiting times. This means that all qubit control pulses can be generated with a single π-pulse envelope with less than 400 samples of waveform data for both channels. This is in contrast to conventional techniques where

patterns for all pulse delays need to be uploaded to the AWG sample-by-sample, which would require waveform data of about 200×(26 µs)×(2 channels)×(1.8 GSa/s)=18.7 MSa and therefore a much longer waveform transfer time.

Qubit Coherence Time

The Ramsey fringe measurement shows the free coherent evolution of the qubit. It provides a measurement of the qubit coherence time. The Ramsey sequence consists of two π/2-pulses separated by a varying delay time followed by a qubit readout. In the absence of decoherence, the two π/2-pulses add up to a full π-pulse and the qubit ends up in the excited state. Dephasing and relaxation during the delay time causes the pulse addition to be imperfect which means the probability for being in the excited state decays with the delay time. Furthermore, a slight detuning of the pulse frequency relative to f_{qb} causes a beating effect between the qubit phase and the phase of the control pulse carrier, resulting in an oscillatory contribution in the readout signal. From the measurement in Fig. 4 (b), we extract a dephasing time of $T_2^* = 1.2$ µs.
The pulses generated by the dual-channel AWG have intermediate-frequency carriers at 112.5 MHz that are generated using the UHF-AWG modulation mode operating in the digital domain. The intermediate frequency is subsequently upconverted to the qubit transition frequency using an analog mixer. Using amplitude modulation means that the carrier frequency and phase can be adjusted or swept without reprogramming the AWG.

Conclusion

This series of essential qubit measurements demonstrates the capabilities of the Zurich Instrument UHFLI lock-in amplifier and AWG in an experimental domain requiring high speed, timing precision, and signal quality. The measurements provide an extensive characterization of a qubit device in terms of its operating frequency, lifetime, and coherence time. Based on the elementary pulses used for these measurements, more complex sequences for experiments such as spin echo or randomized benchmarking are set up in a straightforward manner.

Acknowledgements

Zurich Instruments would like to thank Prof. Wallraff and his team for sharing experimental results and for their strong commitment to developing qubit experiments with Zurich Instruments technology. Special thanks go to Michele Collodo for carrying out the measurements and providing an excellent framework for the integration of the UHFLI into the existing laboratory infrastructure. We thank Theodore Walter for providing the qubit sample and Yves Salathe, Simone Gasparinetti, and Philipp Kurpiers for support with the measurements and for discussions.
This work was supported by the Swiss Federal Department of Economic Affairs, Education and Research through the Commision for Technology and Innovation (CTI).

References

[1] R. P. Feynman. Simulating physics with computers. Int. J. of Theor. Phys., 21:467, 1982.

[2] T. D. Ladd, F. Jelezko, R. Laflamme, Y. Nakamura, C. Monroe, and J. L. O'Brien. Quantum computers. Nature, 464:45, 2010.

[3] Y. Nakamura, Pashkin, Yu. A., and Tsai J. S. Coherent control of macroscopic quantum states in a single-Cooper-pair box. Nature, 398:786, 1999.

[4] John Clarke and Frank K. Wilhelm. Superconducting quantum bits. Nature, 453:1031, 2008.

[5] A. Wallraff, D. I. Schuster, A. Blais, L. Frunzio, R.-S. Huang, J. Majer, S. Kumar, S. M. Girvin, and R. J. Schoelkopf. Strong coupling of a single photon to a superconducting qubit using circuit quantum electrodynamics. Nature, 431:1627, 2004.

[6] M. D. Reed, L. DiCarlo, B. R. Johnson, L. Sun, D. I. Schuster, L. Frunzio, and R. J. Schoelkopf. High-fidelity readout in circuit quantum electrodynamics using the Jaynes-Cummings nonlinearity. Phys. Rev. Lett., 105:173601, Oct 2010.

[7] Jens Koch, Terri M. Yu, Jay Gambetta, A. A. Houck, D. I. Schuster, J. Majer, Alexandre Blais, M. H. Devoret, S. M. Girvin, and R. J. Schoelkopf. Charge-insensitive qubit design derived from the Cooper pair box. Phys. Rev. A, 76:042319, Oct 2007.

[8] David Schuster. Circuit Quantum Electrodynamics. PhD thesis, Yale University, 2007.

Zurich Instruments
Technoparkstrasse 1
CH-8005 Zurich
Switzerland

Phone +41-44-5150410
Fax +41-44-5150419
Email info@zhinst.com
Web www.zhinst.com